JOURNAL OF CATALYSIS 122, 256–270 (1990)

Catalytic Functionalities of Supported Sulfides

VI. The Effect of H_2S Promotion on the Kinetics of Indole Hydrogenolysis

F. E. MASSOTH,[1] K. BALUSAMI, AND JOSEPH SHABTAI[1]

Department of Fuels Engineering, University of Utah, Salt Lake City, Utah 84112

Received May 22, 1989; revised November 3, 1989

The kinetics of concurrent indole hydrogenolysis and naphthalene hydrogenation in the presence of varying concentrations of H_2S were studied in a fixed-bed reactor at 350°C and 35 atm total pressure over a sulfided $CoMo/Al_2O_3$ catalyst. Major reaction products from indole hydrogenolysis consisted of *o*-ethylaniline, ethylcyclohexane, and ethylbenzene, with small amounts of dihydroindole formed in equilibrium with indole. Data were analyzed with Langmuir–Hinshelwood rate equations. It was found that the rate of the first C–N bond-breaking step leading to *o*-ethylaniline depended on the square root of the H_2S partial pressure and was inhibited by indole and dihydroindole. Ring hydrogenation reactions were similarly inhibited, but were little affected by H_2S. The kinetic analyses support the concept that different catalyst sites are involved in the C–N hydrogenolysis and ring hydrogenation reactions.

INTRODUCTION

A number of kinetic studies have been reported on the hydrodenitrogenation (HDN) of quinoline (*1–5*) and indole (*6–8*) over sulfided $CoMo/Al_2O_3$ or $NiMo/Al_2O_3$ catalysts. These studies have shown that the reaction proceeds sequentially in the order: (1) rapid hydrogenation of the *N*-containing ring; (2) hydrogenolytic cleavage of the β C–N bond forming an aromatic amine; and (3) cleavage of the α C–N bond (with or without attendant hydrogenation of the residual carbocyclic aromatic ring) to give hydrocarbons and ammonia. The predominant hydrocarbon product is an alkylcyclohexane, accompanied by smaller amounts of alkylbenzene. It should be appreciated that if in the above reaction sequence a ring hydrogenation (HYD) step is rate-limiting, then the overall HDN (based on hydrocarbon products) may represent HYD rather than C–N bond breaking. It is obvious in such a case that the HDN rate does not necessarily relate to C–N bond hydrogenolysis (CNH). In the present study, the individual C–N bond hydrogenolysis and ring hydrogenation steps involved in the reaction sequence for the hydrogenolysis of indole are separately analyzed to obtain rate expressions for each.

It is well-known that *N*-containing compounds adsorb strongly on sulfided molybdena catalysts. Consequently, the rate of hydrogenolysis is inhibited by reactant, *N*-containing intermediates, and ammonia. Since each step in the overall reaction sequence requires analysis of a complex Langmuir–Hinshelwood rate expression, a complete description of the kinetics of the entire process becomes difficult. An example of the complexity of the analysis is given by Satterfield and Yang (*9*), where 10 individual steps with inhibition terms were considered in treating the HDN kinetics of quinoline; even in this case, several assumptions were needed relative to average adsorption strengths of the various *N*-components present. For this reason, a pseudo first-order treatment is often applied to data obtained at the same feed composition with different reaction times. In such a case, the relative contributions of the individual

[1] To either of whom correspondence should be addressed.

0021-9517/90 $3.00

steps can be approximately assessed. For low conversions, further analysis may be done to relate the pseudo first-order rate constants to the partial pressures of the various species present in order to extract the kinetic parameters and inhibition terms by varying the feed composition (*4, 6*). In the present study, indole was used as a model for the HDN reaction, since the reaction network of this compound is less complex, viz., has fewer intermediates than that of quinoline.

Studies in which the H_2S concentration was varied showed that it had a mild or moderate inhibition on ring hydrogenation, but a strong accelerating effect on C–N bond hydrogenolysis (*1, 2, 10, 11*). The present paper is specifically concerned with a kinetic treatment which quantitatively relates the promotional effect of H_2S on the rate of the C–N bond-breaking reaction, the main objective being to develop an appropriate equation for the H_2S promotional effect.

Much controversy attends the question as to whether only one type of active site or different sites are involved in the different reactions which occur on this catalyst (*12*). This is pertinent to the present study in that both C–N bond hydrogenolysis and ring hydrogenation steps are involved in the HDN of indole, and the particular site requirements should be incorporated in the kinetic analysis. Therefore, a secondary objective of this study was to develop kinetic expressions for the individual reaction steps. To further elucidate the ring hydrogenation reaction per se, naphthalene was added to the indole feed.

EXPERIMENTAL

Catalyst and Experimental Procedure

The catalyst used was Ketjenfine 124-1.5E, which consisted of 3.5% CoO and 12.0% MoO_3 supported on alumina (180 m^2/g). The 1.6-mm extrudates were crushed and sieved to 20- to 40-mesh particles and calcined at 500°C for 16 h.

TABLE 1

Reaction Conditions for Runs with Variable CS_2 Feed

Catalyst (g)	0.50
Temperature (°C)	350
Pressure (atm)	35
Feed rate[a] (ml/h)	5.0–16.7
H_2 rate (cm^3 (STP)/min)	140
Indole pressure (atm)	0.05–0.14
Naphthalene pressure (atm)	0.05–0.13
H_2S pressure (atm)	0.10–1.08
H_2 pressure (atm)	32.1–26.8

[a] Feed: 2 wt% indole, 2 wt% naphthalene, 1.0, 2.0, or 4.0 ml CS_2, balance *N*-heptane.

Kinetic runs were carried out in a fixed-bed reactor (*7*) at 350°C under vapor-phase conditions. A 0.5-g sample of catalyst, mixed with 5 cm^3 of glass beads, was presulfided *in situ* with a 10% H_2S–90% H_2 mixture under atmospheric pressure and 400°C for 2 h. The liquid feed consisted of 2.0 wt% of indole, 2.0 wt% of naphthalene, and either 1.0, 2.0, or 4.0 ml of carbon disulfide, dissolved in *n*-heptane. A constant hydrogen flow of 140 cm^3 (STP)/min was maintained throughout the runs. After aging the catalyst for 2 days under reaction conditions, liquid samples were taken at various liquid flow rates between 5 and 16 ml/h. Product samples were analyzed by gas chromatography on a 0.32 × 366-cm stainless-steel column packed with 6% OV-17 on 100–120 mesh Chromosorb, by use of an FID detector and a temperature programming of 10°C/min. The identity of individual products was determined by comparison with pure reference samples.

Two series of runs were carried out. In one, the same catalyst was used in several runs in which the carbon disulfide concentration was varied. The ranges of reaction conditions used in this series are given in Table 1. In the second series, another catalyst charge was used and the hydrogen pressure was varied. The major organic products of the hydrogenation–HDN reac-

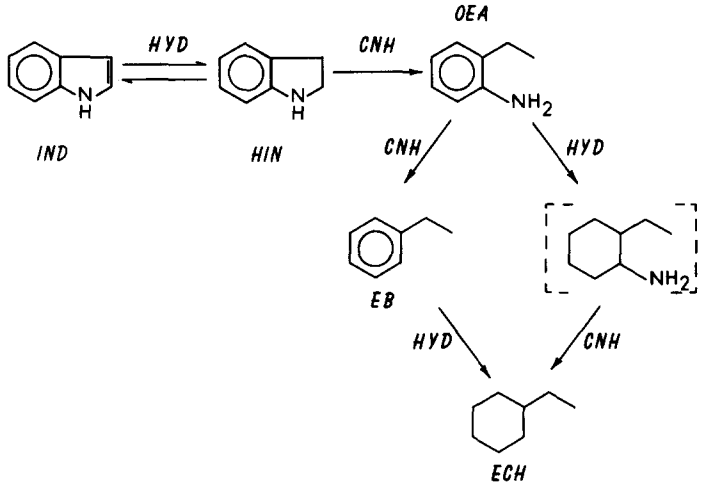

FIG. 1. Reaction network for HDN of indole.

tion were *o*-ethylaniline (OEA),[2] ethylcyclohexane (ECH), and ethylbenzene (EB). Smaller amounts of dihydroindole (HIN), aromatic amines (<3%), and higher molecular weight polymers (<5%) were also formed. Effectiveness factors calculated according to Satterfield (*13*) showed that they were essentially unity under the reaction conditions employed.

[2] List of symbols used: b, ratio of promoted to unpromoted rate constants, atm^{-m}; D, inhibition term; DEC, decalin; ECH, ethylcyclohexane; EB, ethylbenzene; f_{eq}, equilibrium function, Eq. (21); f_H, hydrogen function, Eq. (23); f_s, promotion function, Eq. (9); f'_s, promotion function, Eq. (14); F^m, molar flow rate, mol/h; F_H, hydrogen flow rate, cm^3(STP)/min; F_L, liquid feed rate, ml/h; F_T, total flow rate, cm^3(STP)/min; g, parameter function, Eq. (17) or (24); HIN, 2,3-dihydroindole; IN, indole; k, rate constant, liter/h-g; k', promoted rate constant, liter/h-g-atm^m; k^0, rate constant, liter/h-g-atm; K, adsorption constant, atm^{-1}; K_{eq}, IN–HIN equilibrium constant, atm^{-1}; m, exponent on p_s; n, exponent on D; NAP, naphthalene; OEA, *o*-ethylaniline; p, partial pressure, atm; p^0_A, inlet partial pressure of indole, atm; P, total pressure, atm; r, reaction rate, liter/h-g; S, ECH/EB selectivity; TET, tetralin; V_L, liquid feed molar volume, ml/mol; W_C, catalyst weight, g; x, CNH conversion, Eq. (1); x', HDN conversion, Eq. (2); X, mole fraction; y, NAP conversion, Eq. (6). Subscripts used: A, IN + HIN (also refers to pathways in Fig. 6); AM, NH_3; B, OEA; C, ECH; D, EB; H, H_2; s, H_2S. A, B, C and D also refer to pathways in Fig. 6. Greek symbols used: τ, space time, h-g/liter.

Data Treatment

The reaction network for the HDN of indole (IN) given in Fig. 1 has been previously studied. The conversion of IND to dihydroindole (HIN) is fast, being essentially at equilibrium under the reaction conditions employed (*6–8*). The main intermediate, *o*-ethylaniline (OEA), reacts further by two paths (*8, 14*), viz., direct hydrogenolytic denitrogenation leading to ethylbenzene (EB), or, preferably, ring hydrogenation, followed by fast denitrogenation leading to ethylcyclohexane (ECH). The intermediate, ethylcyclohexylamine, is very reactive and was not observed in the products. The rate-limiting step for formation of ECH is a ring hydrogenation (HYD) rather than a C–N breaking step. The hydrogenation of EB to ECH was negligible under the reaction conditions used.

Since the hydrogenation of indole to dihydroindole is at equilibrium under our reaction conditions, it is convenient to consider both as reactants for the purpose of determining the conversion of the first C–N bond hydrogenolysis (CNH) step. Thus, the CNH conversion, x, is given by

$$x = \frac{X_{OEA} + X_{ECH} + X_{EB}}{\Sigma X_i}. \qquad (1)$$

where X is the mole fraction of hydrocarbon reactant or products as determined by GC analysis. The HDN conversion, x', which includes only hydrocarbon products, is given by

$$x' = \frac{X_{ECH} + X_{EB}}{\Sigma X_i}. \quad (2)$$

The hydrogenation selectivity, S, is defined by

$$S = X_{ECH}/X_{EB}. \quad (3)$$

The mode of operation adopted in the runs involved varying the liquid feed rate while holding the H_2 flow rate constant. Hence, the total gas space velocity varied only slightly (~15%) over the liquid feed rate range studied (since a high ratio of H_2 to liquid feed was employed), whereas the indole partial pressure varied almost proportionally with the liquid feed rate. The space time, τ, is given by

$$\tau = W_c/F_T, \quad (4)$$

where W_c is the catalyst weight (g), and F_T is the total gas flow (cm^3 STP/min). The space time is uniquely determined by the liquid feed flow rate, F_L (ml/h), by the relation

$$F_T = F_H + \frac{22{,}400}{60} F_L/V_L, \quad (5)$$

where F_H is the hydrogen flow rate (constant at 140 cm^3/min) and V_L is the molar volume of liquid feed (taken equivalent to heptane).

Since naphthalene (NAP) was a coreactant with indole, the above equations also apply to the hydrogenation of the former. The reaction products of naphthalene hydrogenation were decalin (DEC) and tetralin (TET). The naphthalene hydrogenation conversion, y, is defined in terms of the overall hydrogenation of the first and second rings in NAP and is given by

$$y = \frac{X_{DEC} + X_{TET}}{\Sigma X_j}, \quad (6)$$

where ΣX_j is the sum of $X_{DEC} + X_{TET} + X_{NAP}$.

RESULTS

A. Course of the Reaction

Variations in reactant (IN + HIN) conversion (x) with liquid feed rate, at three different CS_2 concentrations, are given in Fig. 2. Since the H_2 flow rate was kept constant, the total gas flow rate only changed nominally (about 15%), whereas the concentration of reactant changed appreciably over the range of liquid flow rates. Thus, if the rate of disappearance of reactant was first-order, only a small loss in conversion would be expected as the liquid flow rate increased. The large drop in conversion indicates appreciable inhibition of the reaction due to adsorbed reactant and/or products. A similar effect is noted in the HDN conversion (x'), e.g., conversion to hydrocarbon products.

The observed effect of increasing H_2S (CS_2) in the feed was to increase the conversion of reactant, i.e., to accelerate the β C–N bond hydrogenolysis step, leading to OEA. Overall formation of hydrocarbon products (HDN conversion) was also increased with higher H_2S concentrations (Fig. 2), but to a somewhat lesser extent.

Figure 3 shows the course of the reaction with respect to the OEA intermediate and the hydrocarbon products ECH and EB. The maxima in the OEA curves signify that OEA is a true intermediate in the reaction pathway, whereas the increasing ECH and EB concentrations with increasing conversion are consistent with these being secondary products of the reaction of OEA (Fig. 1). For each run at a different CS_2 feed level, the hydrogenation selectivity ECH/EB ratio was approximately constant, indicating that hydrogenation of EB to ECH was negligible, in agreement with previous results (7). Increase in the level of CS_2 in the feed resulted in higher yields of OEA, lower yields of ECH, and only slightly lower yields of EB (viz., selectivity decreased with increase in CS_2), at the same conversion (Fig. 3). However, at the same space time, both overall conversions

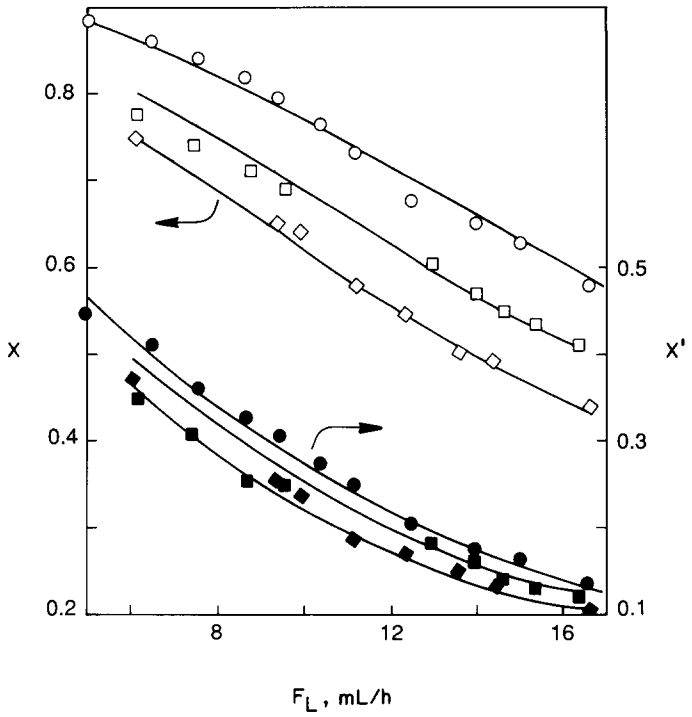

FIG. 2. CHN (×) and HDN (×') conversions vs liquid feed rate. Symbols: (○) 4.0, (□) 2.0, (◇) 1.0 ml CS_2 in 100 ml of liquid feed; open for CNH and solid for HDN.

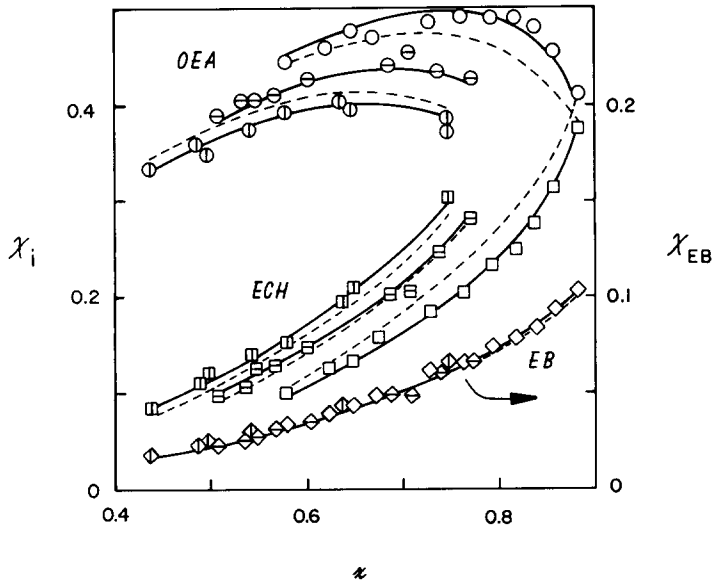

FIG. 3. Product selectivities vs CNH conversion (×). Symbols: (○) OEA, (□) ECH, (◇) EB; (○) 4.0, (⊖) 2.0, (⊕) 1.0 ml CS_2 in feed.

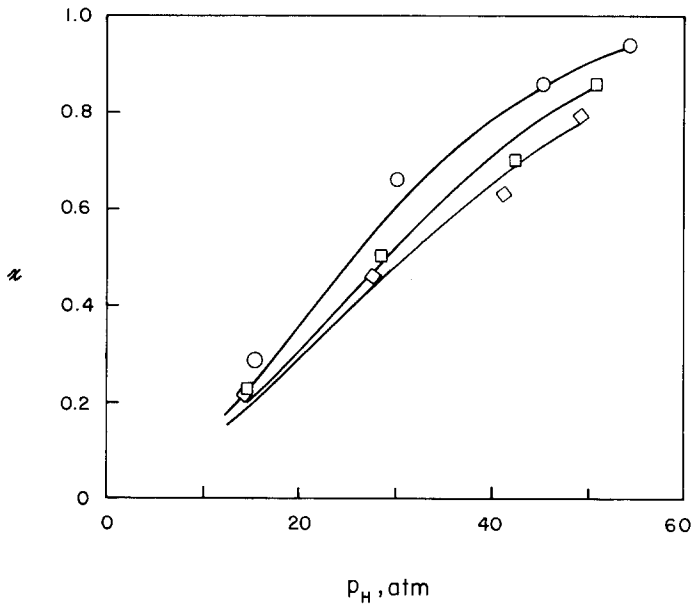

FIG. 4. CHN conversion (×) vs hydrogen partial pressure. Symbols: (○) 8.0, (□) 12.0, (◇) 14.0 ml/h liquid feed rate.

(CNH) and hydrocarbon yields (HDN) increased with increasing H_2S (Fig. 2).

Figure 4 shows the effect of total pressure on CNH conversion at three liquid feed rates. The H_2 pressure is approximately proportional to the total pressure. The results indicate a substantial increase in CNH rate with increasing H_2 pressure.

In Figure 5 is shown the naphthalene hydrogenation conversion during the indole runs as a function of the liquid feed rate. This reaction also shows evidence of reactant/product inhibition. The somewhat higher conversions at higher CS_2 feed levels would seem to indicate a slight promotion of the hydrogenation by H_2S. But as shown later, this is a manifestation of the companion indole conversion rather than a true promotional effect.

B. Kinetics of CNH

1. Preliminary analysis. The kinetics of the reactions involved in the indole network and in concurrent naphthalene hydrogenation were analyzed according to the reaction scheme of Fig. 6. We assume that the first C–N hydrogenolysis step leading to OEA occurs by the energetically easier reaction of HIN, rather than IN. However, since the concentration of HIN was low (in the order of 10% of the total indole concentration), with consequent greater potential error in analysis, and since HIN was in equilibrium with IN, analysis was made on the basis of the sum of IN + HIN in order to improve accuracy.

Preliminary kinetic analysis of the CS_2 series of runs was made assuming constant hydrogen partial pressure (about 18% variation in hydrogen pressure occurred over the feed range used). Since the CNH reaction showed reactant/product inhibition, we adopted a Langmuir–Hinshelwood rate expression of the form

$$-r_A = \frac{k_A X_A}{D_A^n} f_s, \qquad (7)$$

where r_A is the CNH rate, k_A is an apparent rate constant, X_A is the mole fraction, f_s is a function of the hydrogen sulfide partial pressure, D_A is an inhibition term of order n, and subscript A stands for IN + HIN

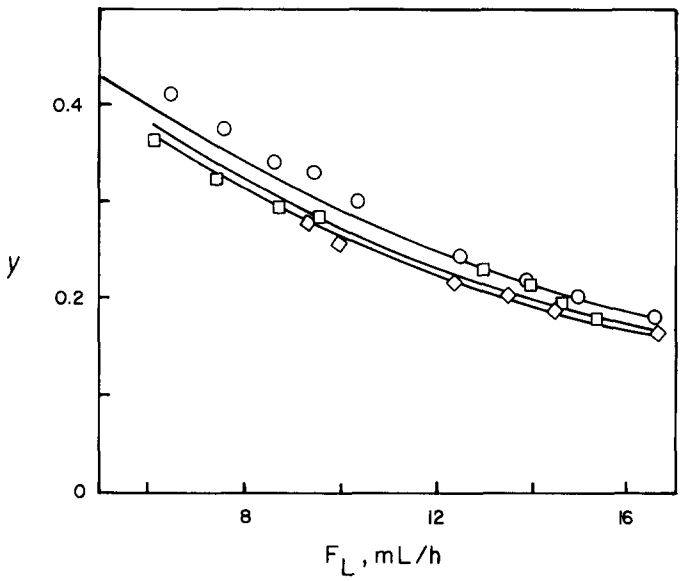

FIG. 5. Naphthalene conversion (y) vs liquid feed rate. Symbols as in Fig. 2.

(Fig. 6). The function f_s accounts for the promotional effect of H_2S on the CNH reaction. In order to develop a relationship for f_s in terms of p_s, consideration must be given to the fact that HDN can occur in the absence of H_2S (*15, 16*). Therefore, we assume reaction can proceed by two paths, one unpromoted and the other promoted by H_2S. We presume the promoted path would be proportional to some power, m, of the H_2S partial pressure. For the overall rate, assuming the same sites are involved, one can formulate

$$-r_A = \frac{k_A X_A}{D_A^n} + \frac{k'_A X_A}{D_A^n} p_s^m = \frac{k_A X_A}{D_A^n}(1 + b_A p_s^m), \quad b_A = k'_A/k_A, \tag{8}$$

where k'_A is the apparent rate constant for the promoted reaction. Comparison of Eqs. (7) and (8) gives

$$f_s = 1 + b_A p_s^m \tag{9}$$

$$D_A = 1 + \Sigma K_i p_i, \tag{10}$$

where K_i is the adsorption constant for each adsorbed specie. As hydrocarbons are relatively weakly adsorbed compared to N-containing compounds, only the latter are considered in the analysis. In terms of conversion of x and x', D_A becomes

$$D_A = 1 + K_A p_A^0(1 - x) + K_B p_A^0(x - x') + K_{AM} p_A^0 x'. \tag{11}$$

Here, p_A^0 is the indole feed partial pressure, K_A is a combined adsorption constant for IN and HIN (see later), K_{AM} is the absorption constant for NH_3, and $p_A^0 x'$ is the ammonia partial pressure (equivalent to $p_{ECH} + p_{EB}$).

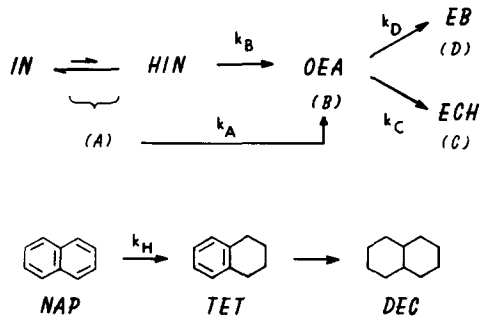

FIG. 6. Reaction scheme for kinetic analysis.

The rate of CNH can now be written

$$\frac{dx}{d\tau} = \frac{k_A(1-x)f_s}{(1 + K_A p_A^0(1-x) + K_B p_A^0(x-x') + K_{AM} p_A^0 x']^n} \quad (12)$$

Solution of Eq. (12) requires a relationship between x' and x. This can be obtained from an analysis of the second C–N bond breaking hydrogenolysis reaction of OEA to EB. Thus, referring to Fig. 6,

$$\frac{dX_D}{d\tau} = \frac{k_D X_B}{D_D^n} \cdot f_s', \quad (13)$$

where the H_2S promotional factor f_s' is given by

$$f_s' = 1 + b_D p_s^m \quad (14)$$

Since $X_D = x'/(1+S)$, Eq. (13) becomes

$$\frac{1}{1+S}\frac{dx'}{d\tau} = \frac{k_D(x-x')}{D_D^n} \cdot f_s'. \quad (15)$$

Assuming the same sites are involved for both C–N bond breaking steps ($D_A = D_D$), division of Eq. (15) by Eq. (12) gives

$$\frac{dx'}{dx} = \frac{k_D f_s'}{k_A f_s}(1+S)\left(\frac{x-x'}{1-x}\right). \quad (16)$$

Solution of this equation gives

$$x' = 1 - x + \frac{g}{1-g}[1 - x - (1-x)^g] \quad (17)$$

$$g = \frac{k_D f_s'}{k_A f_s}(1+S).$$

Finally, incorporation of Eq. (17) into Eq. (12) gives an expression in terms of the two variables x and τ,

$$\frac{dx}{d\tau} = \frac{k_A(1-x)f_s}{[1 + K_A p_A^0(1-x) + K_B p_A^0[x - x(g)] + K_{AM} p_A^0 x(g)]} \quad (18)$$

where $x(g) = x'$ in Eq. (17).

Equation (18) could not be evaluated for best estimates of the parameters by a numerical integration technique because each change in liquid flow gives a different p_A^0 value, i.e., p_A^0 and p_s are not independent of τ. Therefore, it was necessary to integrate Eq. (18) for each individual liquid flow rate in which p_A^0 and p_s are constant. Because of the complexity of the integrated forms obtained, especially for $n = 2$, simplified cases were first evaluated in which certain of the K terms were set equal to zero. By this analysis, it was found that K_A was significant and that K_B and K_{AM} were negligible. Thus, Eq. (18) reduces to

$$\frac{dx}{d\tau} = \frac{k_A(1-x)}{[1 + K_A p_A^0(1-x)]^n} f_s. \quad (19)$$

TABLE 2

Parameter Values from Eq. (19)

n	1	1	2	2
m	1	½	1	½
k_A (liter/h-g)	59.6	44.3	44.6	32.9
b_A (atm^{-m})	0.64	1.12	0.65	1.17
K_A (atm^{-1})	40.8	40.5	9.71	9.70
Rel. error (%)	3.66	2.81	3.71	2.64

Nonlinear least-squares analyses performed on integrated forms of Eq. (19) for $n = 1$ or 2 gave the results listed in Table 2. The objective function, Rel. error, is defined by

$$\text{Rel. error} = 100\sqrt{\frac{\Sigma}{DF}}$$

$$\Sigma = \sum_{i=1}^{N}\left(\frac{Y_i - F_i}{F_i}\right)^2,$$

where Y_i is the experimental value, F_i is the fitted equation value, DF is the degrees of freedom, and N is the number of data points. As can be seen, the cases with $m = \frac{1}{2}$ give the lowest standard deviations, while cases with $n = 1$ or $n = 2$ are not significantly different. For simplicity, the rate form of Eq. (19) with $m = \frac{1}{2}$ and $n = 1$ was chosen for further analysis to include the effect of changing hydrogen pressure. Before this can be done, the effect of hydrogen pressure on the rate must be evaluated.

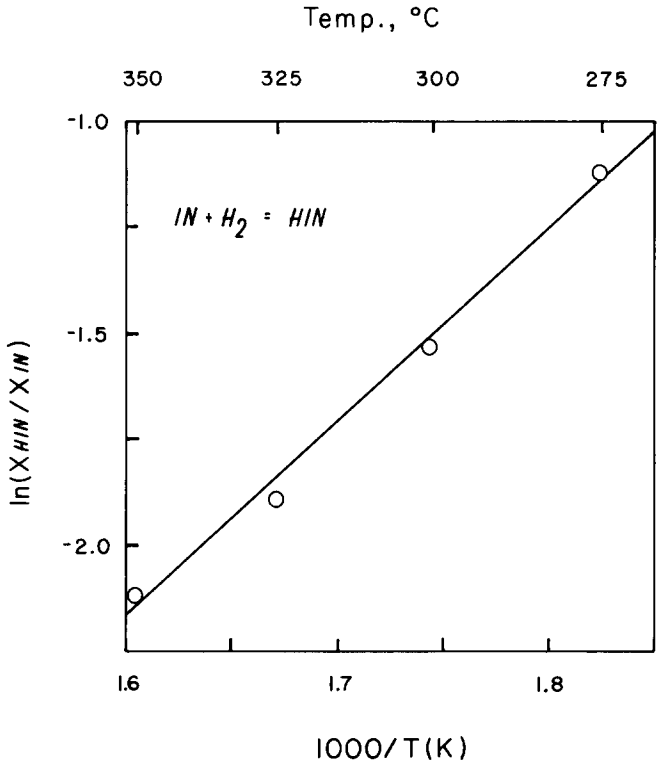

FIG. 7. HIN/IN equilibrium ratio vs temperature.

2. Effect of hydrogen pressure. In order to evaluate the hydrogen pressure effect on the CNH rate, account must be taken of the IN–HIN equilibrium, which is dependent on hydrogen pressure, viz.,

$$\frac{X_{\mathrm{HIN}}}{X_{\mathrm{IN}}} = K_{\mathrm{eq}} p_{\mathrm{H}}, \tag{20}$$

where K_{eq} is the equilibrium constant, and p_{H} is the hydrogen partial pressure. In order to confirm that equilibrium is achieved, separate runs were made with another $CoMo/Al_2O_3$ catalyst at 35 atm total pressure and several temperatures between 275 and 350°C. A plot of the data, given in Fig. 7, shows good conformance to a van't Hoff plot, with a heat of reaction of 9.2 ± 0.5 kcal/mole.

According to the kinetic reaction scheme of Fig. 6, the CNH rate depends on the HIN concentration and the rate constant k_{B}. It is shown in Appendix A that the relationship between k_{A} and k_{B} is given by

$$k_{\mathrm{A}} = k_{\mathrm{B}} f_{\mathrm{eq}}, \quad f_{\mathrm{eq}} = \frac{K_{\mathrm{eq}} p_{\mathrm{H}}}{1 + K_{\mathrm{eq}} p_{\mathrm{H}}}. \tag{21}$$

From measurements of $X_{\mathrm{HIN}}/X_{\mathrm{IN}}$ under various conditions, a value of $K_{\mathrm{eq}} = 4.0 \times 10^{-3}$ atm at 350°C was obtained. The variation of K_{A} with pressure must also be considered. It is shown (Appendix B) that

$$K_{\mathrm{A}} = \frac{K_{\mathrm{IN}} + K_{\mathrm{HIN}} K_{\mathrm{eq}} p_{\mathrm{H}}}{1 + K_{\mathrm{eq}} p_{\mathrm{H}}}. \tag{22}$$

Finally, the variation of k_{B} with p_{H} is to be evaluated, viz.,

$$k_{\mathrm{B}} = k_{\mathrm{B}}^{0} f_{\mathrm{H}}, \tag{23}$$

where k_{B}^{0} is the pressure independent rate constant and f_{H} is a function of p_{H} to be determined. Incorporation of Eqs. (21)–(23) into the rate Eq. (19) for $n = 1$ gives a similar equation where $k_{\mathrm{A}} = k_{\mathrm{B}}^{0} f_{\mathrm{H}} f_{\mathrm{eq}}$ and K_{A} is given by Eq. (22). A satisfactory correla-

TABLE 3

Parameter Values from Eqs. (*19*), (*21*), (*22*), and (*23*)

For $n = 1$ and $m = \frac{1}{2}$ ($K_{eq} = 4.0 \times 10^{-3}$ atm^{-1})	
k_B^0 (liter/h-g-atm)	6.14 ± 1.07
K_{IN} (atm^{-})	8.0 ± 6.9
K_{HIN} (atm^{-1})	50.8 ± 37.6
Rel. error (%)	19.0

tion of this equation was obtained when $f_H = p_H$, i.e., the rate is first-order in hydrogen partial pressure. Parameters obtained from this fit are given in Table 3 and the goodness of fit to the data is shown by the lines in Fig. 4.

Since the objective of the above correlation was to determine the hydrogen pressure effect on the CNH rate constant, k_B, for the CS_2 run series, it can be concluded that first-order in p_H is suitable for correlation purposes. The inclusion of p_H in the rate is necessary for more precise correlation since a variation of about 18% in p_H occurred over the range of liquid feeds employed (Table 1). From the values of K_{IN} and K_{HIN} of Table 3, the variation in K_A over the range of hydrogen pressures was about 9%. However, since K_A appears in the inhibition term, D, its variation has considerably less effect on the rate. Consequently, it was considered a constant in subsequent analyses.

TABLE 4

Parameter Values from Eqs. (*19*), (*21*), and (*22*)[a]

n	1	1[b,c]	2	2
m	1	$\frac{1}{2}$	1	$\frac{1}{2}$
k_B^0 (liter/h-g-atm)	11.0	7.64 ± 0.57	9.93	6.91
b_A (atm^{-m})	0.77	1.44 ± 0.20	0.77	1.46
K_A (atm^{-1})	16.5	16.5 ± 1.7	5.57	5.57
Rel. error (%)	3.87	2.82	4.19	3.12

[a] fs = $1 + b_A p_s^m$, $f_{eq} = K_{eq} p_H/(1 + K_{eq} p_H)$, $K_{eq} = 4.0 \times 10^{-3}$ atm^{-1}.

[b] Equation I of Table 5.

[c] ± are 95% confidence intervals.

3. Kinetics of C–N hydrogenolysis (CNH). Using the integrated forms of Eq. (19) with $k_A = k_B^0 f_{eq} p_H$, best parameter estimates were recalculated for cases with $n =$ 1 or 2 and $m = 1$ or $\frac{1}{2}$. The results are given in Table 4. Again cases with $m = \frac{1}{2}$ gave lowest error, and cases with $n = 1$ or 2 were about equivalent. The case of $n = 1$ and $m = \frac{1}{2}$ was chosen as suitable to represent the CNH kinetics. The resultant equation is given by Eq. I in Table 5. Fit of the data to this equation is shown by the solid lines in the x vs F_L plots of Fig. 2, where a good fit is obtained.

4. Kinetics of hydrodenitrogenation (HDN). Equation (II) of Table 5 gives a rate expression for the HDN reaction. Here we assume the same sites are involved for CNH of OEA as for CNH of HIN (and consequently the same adsorption constant)

TABLE 5

Best Equations Used in Kinetic Analysis

1st CNH: IND → OEA

$$\frac{dx}{d\tau} = \frac{k_B^0 p_H f_{eq} f_s}{D_A} \cdot (1 - x) \qquad \text{(I)}$$

2nd CNH: OEA → EB

$$\frac{dx'}{d\tau} = \frac{k_D^0 p_H f_s'(1 + S)}{D_A} \cdot (x - x') \qquad \text{(II)}$$

$$\frac{dx'}{dx} = \frac{k_D^0 f_s'(1 + S)}{k_D^0 f_{eq} f_s} \cdot \frac{(x - x')}{(1 - x)} \qquad \text{(III)}$$

HYD: OEA → ECH

$$\frac{dx'}{d\tau} = \frac{k_C^0 p_H(1 + S)}{D_C S} \cdot (x - x') \qquad \text{(IV)}$$

$$S = \frac{k_C^0 D_A}{k_D^0 f_s' D_C} \qquad \text{(V)}$$

HYD: NAP → TET + DEC

$$\frac{dy}{d\tau} = \frac{k_H^0 p_H}{D_H} \cdot (1 - y) \qquad \text{(VI)}$$

$$\frac{dy}{dx} = \frac{k_H^0 D_A}{k_B^0 f_{eq} f_s D_H} \cdot \frac{(1 - y)}{(1 - x)} \qquad \text{(VII)}$$

Note. $D_A = 1 + K_A p_A^0(1 - x)$; $D_C = 1 + K_A' p_A^0(1 - x) + K_s' p_s$; $D_H = 1 + K_A'' p_A^0(1 - x)$; $f_s = 1 + b_A \sqrt{p_s}$; $f_s' = 1 + b_D \sqrt{p_s}$; $f_{eq} = \dfrac{K_{eq} p_H}{1 + K_{eq} p_H}$.

TABLE 6

Parameter Values for Eqs. (16) and (17)

k_D^0 (liter/h-g-atm)	0.170 ± 0.019
b_D (atm$^{-1/2}$)	0.342 ± 0.161
Rel. error (%)	5.09

and that the former reaction is also first-order in p_H. Dividing Eq. (II) by Eq. (I) of Table 5 gives Eq. (III), which is similar to Eq. (16) and its integrated form Eq. (17), with

$$g = \frac{k_D^0 f_s'}{k_B^0 f_{eq} f_s}. \tag{24}$$

This equation was solved by nonlinear analysis to give best values of the parameter k_D^0 and b_D from the x, x', and S data, using values of k_B^0 and b_A from Table 4 for $n = 1$ and $m = \frac{1}{2}$. The results, listed in Table 6, show that the rate constant for CNH of OEA to EB (k_D^0) is about 50 times smaller than that for CNH of HIN (k_B^0 of Table 4). Also, the significant value of b_D indicates that the CNH of OEA is promoted by H_2S, in a way similar to the CNH of HIN, but to a lesser extent. The goodness of fit to the data using these parameters and experimental S values is shown by the solid lines in Fig. 2. On the whole, a good representation of the data is obtained.

5. Kinetics of hydrogenation (HYD) of OEA. Two cases need to be considered, viz., (a) the same sites are involved in CNH and ring hydrogenation (HYD), or (b) different sites are operative for the two types of reaction. We assume the HYD reaction is first-order in hydrogen partial pressure. The reaction of *o*-proplyaniline has been reported to be first-order in hydrogen (*3*).

In case (a), from the kinetic scheme of Fig. 6, Eqs. (II) and (IV) of Table 5 apply to the conversion of OEA to EB and ECH, respectively. Dividing Eq. (IV) by Eq. (II) with $D_A = D_c$ gives

$$S = k_c^0/k_D^0 f_s', \tag{25}$$

which shows the hydrogenation selectivity to be only a function of the H_2S partial pressure. Analysis of Eq. (25) gave the value for k_c^0 in Table 7. This rate constant is about five times larger than k_D^0, in line with the high ECH/EB ratios observed.

Equation (25) provides a relationship for predicting S from the appropriate parameters. This equation for S was incorporated into Eq. (17) with Eq. (24) for g to predict values of x' and X_i from x and the appropriate parameters. The data fits are shown by the dotted lines in Fig. 3. It is clear that the assumption of identical sites for CNH and ring hydrogenation gives a rather poor fit to the data.

In case (b), viz., if different sites are involved in the CNH and hydrogenation reaction paths of OEA, then Eq. (V) of Table 5 applies. Here D_c represents the inhibition term with respect to adsorption on the HYD sites where it assumed that only IN and HIN are strongly adsorbed, but the adsorption constant, K_A', could be different from that on the CNH sites. It was also found that a much better fit was obtained by including an adsorption term, K_s', for H_2S adsorption. Best parameters to the data fit of Eqs. (17) and (IV) are listed in Table 7. Data correlation with these values gave the solid lines in Fig. 3. It thus appears that a model involving different CNH and HYD sites is superior to one in which both reactions utilize the same sites (dotted lines of Fig. 3).

6. Kinetics of naphthalene hydrogenation (HYD). In view of the above, the naph-

TABLE 7

Parameter Values for Hydrogenation of OEA to ECH

	$D_A = D_C$	$D_A \neq D_C$
k_c^0 (liter/h-g-atm)	0.82 ± .17	0.86 ± 0.10
Rel. error (%)	5.80	—
K_A' (atm^{-1})		11.6 ± 1.4
K_s (atm^{-1})		0.59 ± 0.11
Rel. error (%)		3.16

TABLE 8

Parameter Values for Hydrogenation of NAP

	$D_A = D_H$	$D_A \neq D_H$
k_H^0 (liter/h-g-atm)	0.435 ± 0.024	0.448 ± 0.019
K_A'' (atm^{-1})	—	19.4 ± 1.6
Rel. error (%)	5.04	4.08

thalene HYD was assumed to occur on separate sites from that of CNH, with inhibition in IN and HIN. The requisite rate equation is given by Eq. (VI) in Table 5. Here the reaction is assumed to be first-order in hydrogen pressure and D_H is given by

$$D_H = 1 + K_A'' p_A^0(1 - x) + K_S'' p_S, \quad (26)$$

where K_A'' represents combined adsorption of IN and HIN, and K_S'' is the adsorption constant for H_2S. Dividing Eq. (VI) by Eq. (I) yields Eq. (VII) of Table 5. Integration and solution of this equation by nonlinear analysis gave the parameters listed in Table 8. K_S'' was found to be negligible in this case. A fit of the data is shown by the solid lines in Fig. 5. Because of the scatter of the data in Fig. 5, a better representation of the data fit is given in Fig. 8, in which the flow rates are eliminated as a variable in the plot. Again the solid lines represent the fit. If the same sites are assumed for CNH and HYD of naphthalene, i.e., $D_A = D_H$, the dotted lines were obtained. This case results in a slightly poorer fit to the data.

DISCUSSION

The primary purpose of this study was to develop the kinetics of the first C–N bond breaking reaction (CNH), in particular to incorporate the promotional effect of hydrogen sulfide on the rate. The analysis shows that the H_2S promotion depends on the square root of the H_2S partial pressure, implying dissociative adsorption of H_2S. This has very significant implications con-

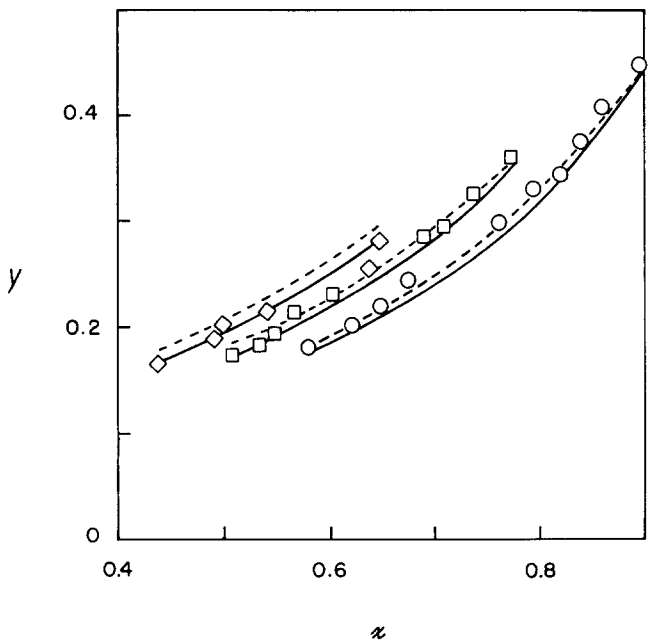

FIG. 8. Naphthalene conversion (y) vs CNH conversion (x). (—) Correlation for $D_A \pm D_Y$; (---) correlation for $D_A = D_Y$. Symbols as in Fig. 2.

cerning the role of H_2S in the mechanism of the HDN reaction occurring at the sulfided catalyst surface, as will be discussed in detail in the subsequent paper of this series. It was also found that the second C–N bond breaking reaction leading from OEA to EB (Fig. 1) is likewise promoted by H_2S, but to a lesser extent, with the result that the overall HDN rate is considerably less promoted than the rate of the first CNH step. Furthermore, the kinetic analysis shows that the CNH steps are strongly inhibited by the N-containing reactants, and only weakly, if at all by the products.

The secondary objective of the study was to kinetically model the hydrogenation reactions of the intermediate OEA and the concurrent hydrogenation of naphthalene to establish whether the same sites are utilized for CNH and HYD reactions. The results, not as clearcut possibly because of larger errors in the data, suggest that separate sites are involved. Overall, the HYD reactions appear to be strongly inhibited by N-containing compounds, particularly HIN and IN.

Indole is rapidly converted to dihydroindole, the reaction being at equilibrium under the reaction conditions employed. This is evident from the good fit of the temperature series (Fig. 7) and the fact that a mixture of IN + HIN gave essentially the same X_{HIN}/X_{IN} ratio (*7*). The equilibrium data are also in good agreement with results of Odebunmi and Ollis (*6*). It is noted in this connection that in the HDN of quinoline, the hydrogenation to 1,2,3,4-tetrahydroquinoline was also found to be essentially in equilibrium (*2, 3*).

We consider that the primary C–N hydrogenolysis step resulting in OEA occurs from HIN rather than from IN, on the basis of the reported bond dissociation energies, i.e., 84 kcal/mol for the (aliphatic)C–N bond vs 105 kcal/mol for the (aromatic)C–N or β (vinylic) C–N bond (*17*). Further, the rate constant found for CNH of the α-bond in OEA (k_D^0) is about 50 times lower than for CNH of the β-bond in HIN (k_B^0), in accordance with the above.

Although kinetic analysis could not distinguish whether the inhibition term D_A should be to the first or second power (Table 4), the first power was adopted for simplicity and the fact that a first-order term has been used by others for quinoline HDN. Our analysis showed only HIN and IN adsorptions to be important, with OEA and NH_3 being relatively weakly adsorbed. An analogous situation was observed for the HDN of quinoline by Giola and Lee (*5*), who found quinoline and 1,2,3,4-tetrahydroquinoline to be the major adsorption inhibitors. On the other hand, Miller and Hinemann (MH4) assumed all N-compounds, except NH_3, were strongly adsorbed for quinoline HDN, while Satterfield and Yang (*9*) modeled their quinoline kinetics with adsorption constants for all N-compounds including NH_3.

No comparative adsorption constants for indole HDN have been reported. However, Satterfield and Cocchetto (*3*) report for quinoline HDN a ratio of $K_{SA}/K_{AA} = 6$, where SA and AA represent secondary amines and aromatic amines, respectively. We may equate HIN to SA and IN to AA, from which we obtain $K_{HIN}/K_{IN} = 6.3$ (Table 3), in good agreement with Satterfield and Cocchetto's value of $K_{SA}/K_{AA} = 6$.

It is evident that OEA undergoes denitrogenation by two parallel pathways, as indicated in Fig. 1. The fact that the selectivity of ECH/EB is essentially invariant with conversion for a given feed, and that EB undergoes only about 5% conversion to ECH when run separately (an even lower conversion would be expected in the presence of indole) indicates that the main HDN pathway involves ring hydrogenation of OEA (to an aliphatic amine) prior to C–N hydrogenolysis, yielding ECH. The increase in ECH/EB selectivity with increase of CS_2 in the feed is additional evidence for separate pathways; i.e., each path is differently affected by H_2S. Furthermore, the equilibrium selectivity of ECH/EB is about 65 under the reaction conditions employed. Since considerably more EB was observed, it is obviously derived

from OEA by a competing but slower pathway, i.e., direct (aromatic)C–N hydrogenolysis.

It has been suggested, on the basis of similarities in CHN and HYD activities for a number of different catalysts, that the same sites are active for both reactions (*7, 18*). However, Giola and Lee (*5*) have claimed these reactions take place on different sites. One may argue for the latter viewpoint on the basis that the CNH reaction is accelerated by H_2S, whereas the HYD reaction is not. On the other hand, both reactions are strongly inhibited by N-compounds. One may envision the same adsorption sites for N-compounds and aromatics, which have adjacent SH groups, the latter promoting the CNH reaction but having no effect on the HYD reaction. Moreau *et al.* (*19*) have presented evidence for two different types of sites, viz., an electron-withdrawing site for hydrogenation and an electron-donating site for heteratom hydrogenolysis.

Our kinetic data are not entirely unequivocal on this question, although most of the data are better explained by assuming two different types of sites for CNH and HYD. The data for HYD of OEA is clearly better assuming different sites, i.e., $D_A \neq D_C$ (solid lines in Fig. 3), than assuming the same sites, i.e., $D_A = D_C$ (dotted lines in Fig. 3), and the range of K'_A values falls outside the range of K_A values. However, the naphthalene HYD analysis yields a K''_A value in the range of the K_A value for CNH analysis (Tables 4 and 8), i.e., $D_A \sim D_H$, and the fit to the HYD data is about as good for this case as for $D_A \neq D_H$ (Fig. 8). Also, the fact that an H_2S adsorption term was needed to obtain good data correlation for HYD of OEA, but not for HYD of NAP, points to differences in adsorption characteristics for these two reactions.

CONCLUSIONS

The salient findings from this study with respect to the reaction conditions employed are:

1. Indole and dihydroindole are in equilibrium.
2. The first C–N bond hydrogenolysis reaction is first-order in H_2 partial pressure and inhibited by indole and dihydroindole. On the basis of a model consisting of a reaction center which is promoted by H_2S, the rate of the promoted reaction is proportional to the square root of the H_2S partial pressure.
3. The second C–N bond hydrogenolysis reaction of *o*-ethylaniline to yield ethylbenzene is also promoted by H_2S, but to a smaller extent.
4. Ring hydrogenation reactions appear to take place on different sites from those for C–N hydrogenolysis reactions.

APPENDIX A: RELATIONSHIP BETWEEN k_A AND k_B

From Fig. 6, at constant hydrogen partial pressure,

$$-\frac{dX_{IN}}{d\tau} = r_1 - r_{-1} \tag{A1}$$

$$-\frac{dX_{HIN}}{d\tau} = \frac{k_B X_{HIN}}{D_A} \cdot f_s - r_1 + r_{-1} \tag{A2}$$

$$X_A = X_{IN} + X_{HIN} \tag{A3}$$

$$-\frac{dX_A}{d\tau} = -\frac{dX_{IN}}{d\tau} - \frac{dX_{HIN}}{d\tau} = \frac{k_B X_{HIN}}{D_A} \cdot f_s. \tag{A4}$$

From equilibrium between IN and HIN,

$$\frac{X_{HIN}}{X_{IN}} = K_{eq} p_H. \tag{A5}$$

Combining Eqs. (A3) and (A5),

$$X_{IND} = \frac{X_A K_{eq} p_H}{1 + K_{eq} p_H} \tag{A6}$$

$$-\frac{dX_A}{d\tau} = \frac{k_B K_{eq} p_H X_A}{(1 + K_{eq} p_H) D_A} \cdot f_s. \tag{A7}$$

Comparison of Eq. (A7) with Eqs. (25) with $X_A = 1 - x$ gives

$$k_A = \frac{k_B K_{eq} p_H}{1 + K_{eq} p_H}, \quad \text{(A8)}$$

which is constant at constant hydrogen pressure and temperature.

APPENDIX B: RELATION BETWEEN K_A, K_{IN}, AND K_{HIN}

The inhibition term in Eq. (A7) is given by

$$D_A = 1 + K_{IN} p_{IN} + K_{HIN} p_{HIN}. \quad \text{(B1)}$$

From Eq. (A5),

$$p_{HIN} = K_{eq} p_H p_{IN}. \quad \text{(B2)}$$

But, $p_A = p_{IN} + p_{HIN}$, from which

$$p_{IN} = \frac{p_A}{1 + K_{eq} p_H} \quad \text{and} \quad p_{HIN} = \frac{K_{eq} p_H p_A}{1 + K_{eq} p_H} \quad \text{(B3)}$$

$$D_A = 1 + \left\{\frac{K_{IN} + K_{HIN} K_{eq} p_H}{1 + K_{eq} p_H}\right\} p_A^0 (1 - x). \quad \text{(B4)}$$

Comparison with Eq. (26) gives

$$K_A = \frac{K_{IN} + K_{HIN} K_{eq} p_H}{1 + K_{eq} p_H}. \quad \text{(B5)}$$

Hence, K_A is dependent upon hydrogen pressure.

ACKNOWLEDGMENTS

The financial support of this work by the U.S. Department of Energy (DE-FG22-83PC60812) is gratefully acknowledged. Thanks are due to the assistance of B. Muegge in obtaining the equilibrium-temperature data.

REFERENCES

1. Shih, S. S., Katzer, J. R., Kwart, H., and Stiles, A. B., *Amer. Chem. Soc. Div. Pet. Chem. Prepr.* **22,** 919 (1977).
2. Bhinde, M. V., Shih, S., Zawadski, R., Katzer, J. R., and Kwart, H., *in* "Third Climax Intern. Conf. Chemistry and Uses of Molybdenum" (B. F. Barry and P. C. H. Mitchell, Eds.), p. 184. Climax Molybdenum Co., Ann Arbor, MI, 1979.
3. Satterfield, C. N., and Cocchetto, J. F., *Ind. Eng. Chem. Proc. Des. Dev.* **20,** 53 (1981).
4. Miller, J. T., and Hineman, M. F., *J. Catal.* **85,** 117 (1984).
5. Giola, F., and Lee, V., *Ind. Eng. Chem. Processes Des. Dev.* **25,** 918 (1986).
6. Odebunmi, E. O., and Ollis, D. F., *J. Catal.* **80,** 76 (1983).
7. Lui, Y., Massoth, F. E., and Shabtai, J. S., *Bull. Soc. Chim. Belg.* **93,** 627 (1984).
8. Olive, J.-L., Biyoko, S., Moulinas, C., and Geneste, P., *Appl. Catal.* **19,** 165 (1985).
9. Satterfield, C. N., and Yang, S. H., *Ind. Eng. Chem. Process Des. Dev.* **23,** 11 (1984).
10. Satterfield, C. N., and Gultekin, S., *Ind. Eng. Chem. Process Des. Dev.* **20,** 62 (1981).
11. Shabtai, J., Yeh, G. J. C., Russel, C., and Oblad, A. G., *Ind. Eng. Chem. Res.* **28,** 139 (1989).
12. Massoth, F. E., and Muraldihar, G., *in* "Fourth International Conf. on Chemistry and Uses of Molybdenum" (H. F. Barry and P. C. H. Mitchell, Eds.), p. 343. Climax Molybdenum Co., Ann Arbor, MI, 1979.
13. Satterfield, C. N., "Mass Transfer in Heterogeneous Catalysis." Colonial Press, MA, 1977.
14. Stern, E. W., *J. Catal.* **57,** 390 (1979).
15. Sonnemans, J., and Mars, P., *J. Catal.* **31,** 209 (1973).
16. Ledoux, M. J., Puges, P. E., and Maire, G., *J. Catal.* **76,** 285 (1982).
17. Benson, S. W., "Thermochemical Kinetics," p. 309. Wiley, New York, 1969.
18. Shabtai, J. S., Guohe, Q., Balusami, K., Nag, N. K., and Massoth, F. E., *J. Catal.* **113,** 206 (1988).
19. Moreau, C., Aubert, C., Durand, R., Zmimita, N., and Geneste, P., *Catal. Today* **4,** 117 (1988).